Chapter 5

Differential Evolution and MAES for Power Flow Problem of Droop Controlled Islanded Microgrids

5.1 Introduction

Conventional PF algorithms are not effective in analyzing the of islanded microgrid as the system frequency and voltage of the slack bus is assumed to be constant. Such assumptions are not applicable in the operation of islanded microgrid as DGs provide the real and reactive power to adjust the load demands as well as maintain the voltage magnitude and system frequency in the absense of the main grid. To solve the power flow of islanded microgrid, a novel formulation as a constrained optimization problem is proposed in this thesis.

A MG has been recognized as a collection of DGs which are interconnected with thermal and electrical loads, and energy storage units. In addition, it functions as a single small scale low-voltage distribution system. Due to the use of power electronic controls and interfaces in MGs, system reliability, security, and power electronic controls can be enhanced [177, 178]. An MG may run in islanded or grid-connected mode. In an islanded mode, controllers of DGs are capable of voltage and frequency regulation along with controlling active and reactive power. While in a grid-connected mode the frequency and voltages of MGs are managed by the main grid.

In practice, different type of control strategies for MGs have been proposed such as

distributed, decentralized, and centralized; any hybrid structure of these models is also feasible. Strategies based on centralized control need to transfer data using stable communication environment. In the case of large MGs, these strategies are not suitable where DGs are placed far from each other [179–181]. Large MGs are usually controlled using decentralized strategies, such as DCIMGs, where communication of significant information is not needed [178]. In droop controller based strategies, local variables can be utilized for effective sharing of loads of loads among DGs. Here, the frequency and magnitude of the voltage of MGs are used as local variables [182].

In DCIMGs, DGs are connected to MGs using suitable control approach using power electronic converters [183–186]. For designing the effective and efficient control strategy, a power flow analysis model is required to calculate the steady-state variables, especially for an islanded MGs. Design of droop control strategies use power flow solutions to test its efficacy. This is more so in the case of MGs operated in islanded mode.

To address the characteristics of MGs and distribution systems, a number of methods have been introduced for PF analysis. Some of such algorithms are derived from the NR approach [23, 43], while others are based on the basic electric circuit laws [51]. In [187], a modified algorithm, called BFS method, has been proposed for solving the power mismatches equations of radial power systems. In [27], an implicit ZBus algorithm based on the superposition principle of electric circuits is proposed to solve the power flow problem.

In [56], a model of three-phase PF problem is proposed which adopt the real characteristics of islanded MGs similar to three-phase distribution systems. In the model proposed in [56], the problem is formulated as a non-linear optimization problem and this problem is solved by NTR technique. But, it is highly sensitive to the initial solutions of variables of the PF problem. In addition, a number of studies of PF analysis for droop controlled islanded MGs based on a nature-inspired optimization algorithm have been developed.

In general, Jacobian based PF algorithms, such as NR, and FD may not produce PF solution for power mismatch equations of distribution systems having a high value of R/X. To solve this problem, a number of methods [183–186] have been introduced. In addition, to present an adequate platform for PF analysis, modeling of distributed slack bus has also been studied [28, 53, 100].

In current practices, DG having the highest capacity is considered as a slack bus which operates like an infinite bus at a constant voltage to provide system frequency, and other DGs are treated as either PV or PQ buses. However, this assumption cannot be considered feasible in the case of islanded MGs. For example, the generation capacity of DGs in MGs is not usually high enough to allow them to act as an infinite bus. In addition, voltage swelling may occur in the buses of MG when a DG is acting as a slack bus. In such a situation, slack bus (DGs) must provide power independently for the whole power losses of MG which is not an effective state of operation for MG [43]. Therefore, in an islanded MG, considering a DG as a slack bus is not appropriate for PF analysis.

In order to resolve this issue, one way is to consider that all DG units operate using droop controllers where all DGs locally tune the voltage and frequency of islanded MG [179]. In such operation, active power generation and voltage magnitude of each DG is required to be fixed according to droop characteristics of controllers. This operation of MG creates a new type of bus, called droop bus, in addition to PQ and PV buses in the system. It is worth to note here that grid-connected MG behaves like a simple distribution system having a slack bus operating as a infinite bus. Other problems related to power flow analysis of islanded MGs can be outlined as dealing with the reactive power scheduling of DGs, and singularity of the Jacobian matrix which causes failure in convergence of PF [185].

In order to resolve these issues, this thesis proposes a new PF formulation for islanded microgrids. This formulation is expressed in form of constrained optimization problem which models different mode of operations of DGs (such as PV, PQ, and droops operations). In order to solve this constrained optimization problem, two novel optimization algorithms are proposed.

The main contributions of this chapter are summarized as follows.

- It introduces a novel formulation as a constrained optimization problem for PF analysis of islanded MGs.
- It proposes PF constraint based on the droop characteristics of distributed slack buses to deal with the droop buses in power flow analysis. In addition, system frequency is also considered as an extra variable of the PF problem.
- It provides an adequate method to share reactive and active power among DGs

based on the droop characteristics in the PF analysis.

- It provides the PF solutions for the islanded MGs using the proposed optimization algorithms.

This chapter is organized as follows. In the second section, the microgrid system and load are modeled. This is followed by formulating the constrained optimization problem for power flow analysis of islanded MGs. In the fourth section, the main steps of the optimization algorithm are proposed. Finally, the validation of the proposed algorithm on the power flow problem of islanded MGs is discussed.

5.2 Modelling of Droop Controlled Microgrid

5.2.1 Modeling of Frequency and Voltage Dependent Loads

Generally, loads are assumed to be independent of the value of voltage and therefore, the active and reactive power demands of loads are treated as constant parameters. However, such premises are not true in practice, especially in MGs where power demand of some loads are depended on the values of frequency and voltages. Mathematically, voltage-dependent loads can be defined as

$$P_l = P_{l,0}\left(\frac{V}{V_0}\right)^{\alpha}, \tag{5.1}$$

and

$$Q_l = Q_{l,0}\left(\frac{V}{V_0}\right)^{\beta} \tag{5.2}$$

where $Q_{l,0}$ and $P_{l,0}$ represent the reactive and active power, respectively, at nominal voltage; Q_l and P_l represent reactive and active power respectively, at operating voltage; V and V_0 represent the magnitude of voltage and nominal voltage, respectively, at load buses; β and α represent the exponent parameters for reactive and active powers, respectively, for the model [188].

In similar way, frequency dependent load can be defined as

$$P_l = P_{l,0}\left(\frac{V}{V_0}\right)^{\alpha}(1 + k_{pf}\triangle f) \tag{5.3}$$

and

$$Q_l = Q_{l,0}\left(\frac{V}{V_0}\right)^{\beta}(1 + k_{qf}\triangle f) \tag{5.4}$$

where $\triangle f$ is the deviation in system frequency with respect to the nominal frequency; k_{qf} and k_{pf} represent frequency dependent parameter, where their values are defined in range $(-2, 0)$ and $(0, 3)$, respectively [189].

5.2.2 Modeling of Lines in Islanded MGs

Line impedance of islanded MGs can be defined as, $z = r + jx(w)$ where, r and x represent the resistance and reactance of the line, respectively. Here, the value of reactance, x, depends on the operating frequency. Therefore, small deviation in frequency can change the reactance of the lines.

5.2.3 Modeling of DGs in Islanded MGs

In grid-connected MGs, DGs can operate to provide pre-specified active and reactive generation to satisfy the power demands of system loads. In such operation, the difference in total load demand and power generated by DGs are supplied or absorbed by the main grid to keep the system frequency and voltages of the buses constant. Similar to conventional power systems, in grid-connected MGs, DGs can be modeled as a PV and PQ bus [190, 191]. However, this cannot be valid in the case of islanded MGs, as shown below:

1. There is no slack bus in islanded MGs.
2. System frequency is not consant.
3. Reference voltage does not exist in islanded MGs to calculate the voltage of all system buses.
4. In an islanded mode, the deviation between power generation and demands may be fixed by changing the system frequency and magnitude of the voltage using droop controllers.

Therefore, the power flow problem of islanded MGs will be solved without considering the slack bus in the system. In order to formulate the PF problem of islanded MGs, in place of a slack bus, multiple droop buses are modeled based on the droop characteristics to share the power demand among the DGs. According to the droop characteristics of

the controllers, an increment in reactive power and active power demand follows from a decrement in magnitude of the voltage and operating frequency, respectively. So, in the case of droop bus, reactive and active power generation of a DG can be calculated using the following equations.

$$P_i = \frac{1}{np_i}(w_i^* - w) \tag{5.5}$$

$$Q_i = \frac{1}{mq_i}(V_i^* - V_i) \tag{5.6}$$

where V_i^* and w_i^* represent the nominal values of voltage magnitude and frequency, respectively; mq_i and np_i represent the reactive and active power static droop gains, respectively.

Based on the IEEE Standard 1547.7 [184], equations (5.5) and (5.6) are valid for islanded MGs where the output impedance of converter is assumed inductive. Figures (5.2) and (5.4) show the sharing of active and reactive power among the DGs.

5.3 Power Flow Formulation

In general, four variables are involved in a conventional power flow viz. active power, reactive power, voltage magnitude, and voltage angle. In the case of PQ bus, the value of voltage angle and voltage magnitude are unknown. In case of PV bus, voltage magnitude and reactive power are unknown. But, in the case of droop bus, all these variables are unknown. Conventional techniques cannot be applied to the power flow problem of islanded MGs as a frequency is not considered constant. In islanded MGs, the operating frequency is also an unknown variable for the power flow problem. Therefore, new equations should be derived for the PV, PQ, and droop buses are presented in the following section.

5.3.1 Modeling of Droop Bus

The value of active and reactive power injection of bus i can be defined as

$$P_i = P_{i,dg} - P_{i,l} \tag{5.7}$$

$$Q_i = Q_{i,dg} - Q_{i,l} \tag{5.8}$$

where, $P_{i,dg}$ and $Q_{i,dg}$ are calculated using equations (5.5) and (5.6). Here, P_i and Q_i can be calculated using following equations.

$$P_i = V_{ri}\sum_{j=1}^{N}(V_{rj}G_{ij} - V_{mj}B_{ij}) + V_{mi}\sum_{j=1}^{N}(V_{rj}B_{ij} + V_{mj}G_{ij}) \tag{5.9}$$

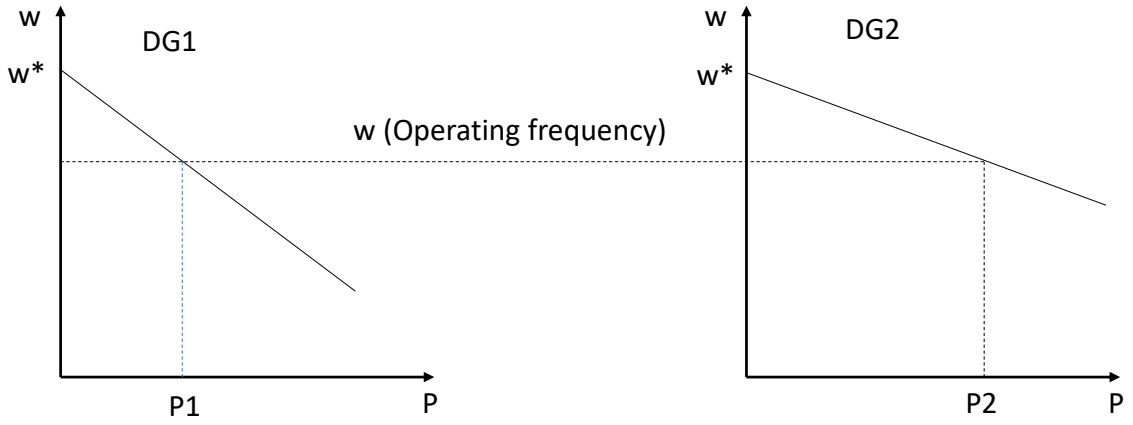

Figure 5.1: Sharing of active power among DGs using droop based controller

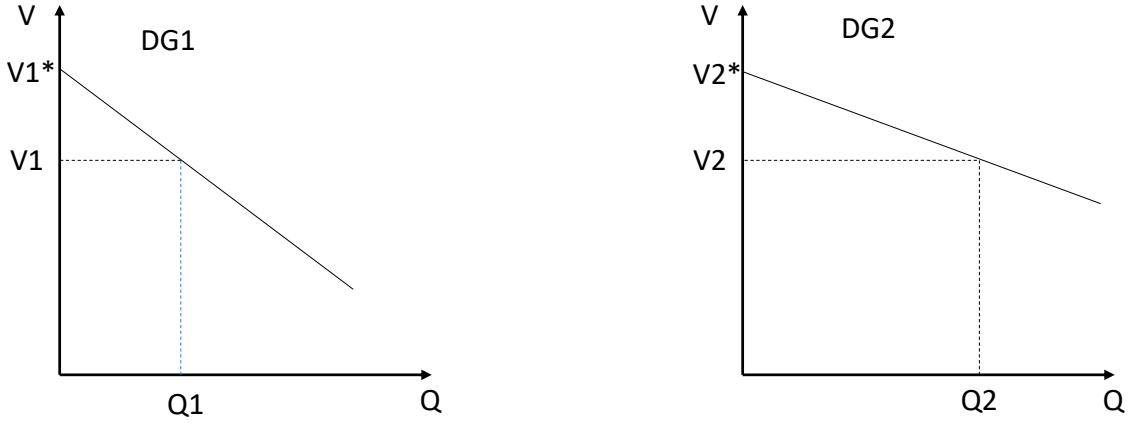

Figure 5.2: Sharing of reactive power among DGs using droop based controller

$$Q_i = V_{mi}\sum_{j=1}^{N}(V_{rj}G_{ij} - V_{mj}B_{ij}) - V_{ri}\sum_{j=1}^{N}(V_{rj}B_{ij} + V_{mj}G_{ij}) \tag{5.10}$$

Power flow equations for droop bus can be derived using equations (5.5), (5.6), (5.7), (5.8), (5.9), and (5.10), which are given below.

$$\frac{1}{np_i}(w_i^* - w) - P_{i,l} = V_{ri}\sum_{j=1}^{N}(V_{rj}G_{ij} - V_{mj}B_{ij}) + V_{mi}\sum_{j=1}^{N}(V_{rj}B_{ij} + V_{mj}G_{ij}) \tag{5.11}$$

$$\frac{1}{mq_i}(V_i^* - V_i) - Q_{i,l} = V_{mi}\sum_{j=1}^{N}(V_{rj}G_{ij} - V_{mj}B_{ij}) - V_{ri}\sum_{j=1}^{N}(V_{rj}B_{ij} + V_{mj}G_{ij}) \tag{5.12}$$

5.3.2 Modeling of PQ Bus

The active and reactive power injection are known in PQ buses, so PQ buses can be defined by following equations

$$P_k = V_{rk}\sum_{j=1}^{N}(V_{rj}G_{kj} - V_{mj}B_{kj}) + V_{mk}\sum_{j=1}^{N}(V_{rj}B_{kj} + V_{mj}G_{kj}) \tag{5.13}$$

$$Q_k = V_{mk}\sum_{j=1}^{N}(V_{rj}G_{kj} - V_{mj}B_{kj}) - V_{rk}\sum_{j=1}^{N}(V_{rj}B_{kj} + V_{mj}G_{kj}) \tag{5.14}$$

5.3.3 Modeling of PV bus

The active power and voltage magnitude are known in PV buses, so PV buses can be defined as given below

$$P_k = V_{rk}\sum_{j=1}^{N}(V_{rj}G_{kj} - V_{mj}B_{kj}) + V_{mk}\sum_{j=1}^{N}(V_{rj}B_{kj} + V_{mj}G_{kj}) \tag{5.15}$$

$$V_k^2 = V_{rk}^2 + V_{mk}^2 \tag{5.16}$$

To solve this proposed power flow formulation, a constrained optimization problem shall be discussed later in the chapter to optimize objective function corresponding to power flow.

5.3.4 Objective Function

The objective function can be formulated as the sum of square error of mismatch equations of droop bus (equations (5.11) and (5.12)) i.e.

$$\text{Minimize, } f = \sum_{k\epsilon S_{dr}}(\triangle P_k^2 + \triangle Q_k^2) \tag{5.17}$$

where

$$\triangle P_i = \frac{1}{np_i}(w_i^* - w) - P_{i,l} - V_{ri}\sum_{j=1}^{N}(V_{rj}G_{ij} - V_{mj}B_{ij}) - V_{mi}\sum_{j=1}^{N}(V_{rj}B_{ij} + V_{mj}G_{ij}) \quad (5.18)$$

and

$$\triangle Q_i = \frac{1}{mq_i}(V_i^* - V_i) - Q_{i,l} - V_{mi}\sum_{j=1}^{N}(V_{rj}G_{ij} - V_{mj}B_{ij}) + V_{ri}\sum_{j=1}^{N}(V_{rj}B_{ij} + V_{mj}G_{ij}) \quad (5.19)$$

The objective function, defined in equation 5.17, has $(2 \times N + 1)$ variables. This objective function is to be optimized subject to following constraints.

1. Equality constraints related to k-th PQ bus:

$$P_k - V_{rk}\sum_{j=1}^{N}(V_{rj}G_{kj} - V_{mj}B_{kj}) - V_{mk}\sum_{j=1}^{N}(V_{rj}B_{kj} + V_{mj}G_{kj}) = 0 \quad (5.20)$$

   and

$$Q_k - V_{mk}\sum_{j=1}^{N}(V_{rj}G_{kj} - V_{mj}B_{kj}) + V_{rk}\sum_{j=1}^{N}(V_{rj}B_{kj} + V_{mj}G_{kj}) = 0 \quad (5.21)$$

2. Equality constraints related to k-th PV bus:

$$P_k - V_{rk}\sum_{j=1}^{N}(V_{rj}G_{kj} - V_{mj}B_{kj}) - V_{mk}\sum_{j=1}^{N}(V_{rj}B_{kj} + V_{mj}G_{kj}) = 0 \quad (5.22)$$

   and

$$V_k^2 - V_{rk}^2 - V_{mk}^2 = 0 \quad (5.23)$$

3. Bound constraints:

$$V_{k,min} \leq V_k \leq V_{k,max} \quad (5.24)$$

   and

$$w_{min} \leq w \leq w_{max} \quad (5.25)$$

In the later sections, two novel constrained optimization algorithms are discussed which have been used to solve the above-mentioned objective for corresponding to power flow problem.

5.4 Differential Evolution with Gauss-Newton based Mutation

The DE [132] algorithm is a popular global optimization technique used in different problems of the power system. The DE relatively more robust and efficient technique as compared with other evolutionary algorithms. Several latest variants of DE have been judged as top-ranked algorithms in recent IEEE congress on evolutionary computation competitions [122, 192]. However, DE may not be directly applied to the constrained optimization problem. A constraint handling technique is required to evaluate the fitness of the solutions on the basis of feasibility and objective function value. In this chapter, epsilon-based constraint handling technique [146] has been employed with the operators of DE to solve the constrained optimization problems. In addition, it is also challenging for EAs to determine a feasible solution for a constrained problem with many equality constraints. For handling the equality constraints, most of the EAs convert equality constraints into relaxed inequality constraints. As a result, the feasibility of the obtained solutions is inadequate. In order to address this issue, this thesis introduces an algorithm to solve the problem with many equality constraints by introducing a Gauss-Newton (GN) based mutation operator that finds a feasible solution from an infeasible solution using the GN [193] algorithm. The proposed algorithm is named as ϵDE-GN and main operators of ϵDE-GN are summarized in the following sub-sections.

5.4.1 Differential Evolution

DE is a search-based global optimization algorithm proposed by Storn and Price [132]. DE can be applied to different type of optimization problems viz. Non-convex, non-differentiable, non-linear and multi-modal problems. In literature, it is shown that DE is robust and efficient on these types of problems. In DE, initial solutions are generated randomly within the lower and upper bound of search space and these solutions form an initial population. Each solution consists of n elements as decision parameters of the problem. At each iteration, all solutions of the population are selected as parents. Offspring generation for each parent is done as follows. The mutation process begins with the random selection of 3 solutions (different from the parent) from the population. The first solution out of 3 is considered as base vector. Other two solutions are utilized

to generate a difference vector. The difference vectors are weighted using parameter s_F and added to the base vector. The resulting solution is then passed through a process of crossover with parent solution. The probability of crossover is guided using a parameter CR (Crossover Rate). The crossover scheme returns a trial solution. Finally, for selection of solution for the next iteration, the trail solution is accepted if the trail vector is better than the parent. In algorithm ϵDE-GN, an exponential crossover is implemented. Another variant of crossover, Binomial Crossover, has been studied well in literature. However, exponential crossover performs better in constrained optimization problem as compared to binomial crossover. Hence, the exponential crossover is adopted in this work.

5.4.2 Gauss-Newton Mutation

The GN mutation is an operator used to calculate a feasible solution for an infeasible solution using gradient information of constraints, $\nabla C(x)$. The constraint vector, $C(x)$, the constraint violation vector, $\triangle C(x)$, and increment expected in point x, $\triangle x$, to satisfy constraints are related in the following manner [193]:

$$\triangle x = -\frac{\nabla C(x)^T \triangle C(x)}{\nabla C(x)^T \nabla C(x)} \tag{5.26}$$

where,

$$\triangle C(x) = [\triangle g_1(x)...\triangle g_n(x), \triangle h_{n+1}(x)...\triangle h_m(x)]^T, \triangle g_i(x) = max\{0, g_j(x)\} \tag{5.27}$$

The relation 5.26 is utilized whenever an infeasible solution, x^{infea}, is encountered. This mutation operation, $x^{fea} = x^{infea} + \triangle x$, is executed where x^{infea} is an infeasible solution.

5.4.3 ϵ-Constrained Handling Technique

In ϵ-constraint handling technique establishes an ϵ-level comparison to compare the solutions [146]. The ϵ-level comparison is defined using lexicographic order in which constraint violation, $\phi(x)(= \sum_{i=1}^{m} \triangle C_i(x))$, precedes objective function value, $f(x)$ as described in following paragraph [146].

Let $\{\phi_1, \phi_2\}$ and $\{f_1, f_2\}$ be the constraint violation value and the function values at points $\{x_1, x_2\}$ respectively. Then, the ϵ level comparisons are defined as follows:

$$(f_2, \phi_2) <_\epsilon (f_1, \phi_1) \Leftrightarrow \begin{cases} f_2 < f_1, & \text{if } (\phi_1, \phi_2 \leq \epsilon) \text{ or } (\phi_1 == \phi_2) \\ \phi_2 < \phi_1, & \text{otherwise} \end{cases} \tag{5.28}$$

$$(f_2, \phi_2) \leq_\epsilon (f_1, \phi_1) \Leftrightarrow \begin{cases} f_2 \leq f_1, & \text{if } (\phi_1, \phi_2 \leq \epsilon) \text{ or } (\phi_1 == \phi_2) \\ \phi_2 \leq \phi_1, & \text{otherwise} \end{cases} \tag{5.29}$$

Generally, ϵ level may not be controlled for most of the constrained optimization problems. However, constrained problems with equality constraints should be solved using controlled ϵ level. A simple way to control the ϵ-level is proposed in [146], which is defined using following equations.

$$\epsilon(t) = \begin{cases} \phi(x_\theta)(1 - \frac{t}{T_c})^{cp}, & 0 < t < T_c \\ 0, & T_c \leq t \end{cases} \tag{5.30}$$

where x_θ represents the top $\theta-$th individuals and cp represent parameter to control the speed of reduction of the ϵ-level.

5.4.4 The Algorithm: ϵDE-GN

The algorithm ϵDE-GN is based on DE/rand/1/exp [146]. The main steps of algorithm ϵDE-GN are as follows.

- **Step 1:** *Initialization*- In this step, initial population, P^0, of N_p solutions is initialized within the bound of search-space using following equation.

$$x_i^0 = (x_U - x_L)rand + x_L, \ i = 1, 2, ...N \tag{5.31}$$

  where x_U and x_L are the upper and lower bounds of search space respectively and *rand* represents the random number from uniform distribution within the range $(0, 1)$. An initial value of $\epsilon-$level, $\epsilon(0)$, is calculated using equation (7.18).

- **Step 2:** *Mutation*- For each solution x_i^k, three different solution x_{r1}^k, x_{r2}^k, and x_{r3}^k are selected from population, P^k, at k-th iteration. A new mutant solution, v_i^k, is calculated using x_{r1}^k, x_{r2}^k, and x_{r3}^k as follows.

$$v_i^k = x_{r1}^k + s_F(x_{r2}^k - x_{r3}^k), \text{ where } (r1 \neq r2 \neq r3 \neq i) \tag{5.32}$$

  where sF is a parameter called scaling factor.

- **Step 3:** *Crossover*- The mutant solution v_i^k, is used as a donor solution in crossover operation for solution x_i^k to generate a trial solution, u_i^k. A crossover point, l, is randomly selected from 1 to D, where D is the dimension of the problem. The element

corresponding $l-th$ dimension of the trail solution u_i^k is taken from the element corresponding to $l-th$ dimension of donor solution v_i^k. Subsequent elements of trial solution u_i^k are taken from donor solution v_i^k with exponentially decreasing probability (calculated using crossover rate CR). Rest of the elements of trial solution u_i^k are taken from the elements of solution x_i^k.

- **Step 4:** *Gauss-Newton Mutation-* If the generated trial solution u_i^k is infeasible (does not satisfy the all constraint), u_i^k is updated using GN. This process is repeated until the number of trials of GN reaches to N_{gn} or solution u_i^k becomes feasible solution. If after N_{gn} number of trials, infeasible trail solution does not become feasible the trial infeasible solutions is discarded in favor of previous feasible solution.

- **Step 5:** *Selection-* If the trial solution u_i^k is better than solution x_i^k on the basis of $\epsilon-$ level comparison, the trial solution u_i^k replaces the solution x_i^k for the next iteration.

- **Step 6:** $\epsilon-$ *level control-* The value of $\epsilon-$ level is updated using equation (7.18).

- **Step 7:** *Termination Condition-* If the total number of iteration becomes greater than maximum allowed iteration (T_{max}), the algorithm is terminated. Otherwise go to **Step 2**.

The performance of ϵDE-GN has been validated on benchmark problems and reported in Appendix-III.

5.5 Matrix Adaptation Evolution Strategy

The performance of Evolutionary Algorithms (EAs) can be heavily undermined in case of COPs where several constraints limit the feasible regions. For example, CMA-ES, one of the most efficient algorithms for unconstrained optimization, cannot readily be extended to solve COPs. Although some attempts of adopting CMA-ES for COPs have been made [156, 157], it is not yet competitive on these types of problems as compared to other popular algorithms like DE, GA, and PSO. There are two main reasons behind the relatively bleaker performance of CMA-ES on COPs: (i) conventional recombination approach of the algorithm cannot be suitable for the search space of COPs due to the

ranking of solutions based on the objective function value and (ii) the self-adaptation of the parameters of the algorithm is not suitable for COPs due to lower volume of the feasible region in search space especially in case of COPs involving several equality constraints.

To overcome these limitations of CMA-ES, we introduce here (i) a constraint handling technique, called υ-level penalty function to modify the fitness value of solutions while ranking the solutions in the algorithm and (ii) a solution repair scheme, called Broyden-based mutation, to handle the feasibility issue of solutions during the optimization process.

Firstly we introduce the υ-level penalty function and Broyden based mutation, then the main steps and framework of the proposed algorithm are discussed.

To solve the COPs, a new constraint handling technique called υ-level penalty function, is proposed in this section.

5.5.1 υ-level Modification in Constraints

Although, ϵ-level comparison of ϵ-constrained method shows good performance as a constraint handling technique with several EAs on COPs [1,146,194], its capability of relaxing infeasible solutions is more prominent in case the solutions violate a lower number of constraints as compared to the situation when several constraints are violated (as illustrated in Figure 5.3). The relaxed feasible region can be represented using Eqn. 5.33.

$$\phi(x) \leq \epsilon \implies \phi(x) - \epsilon \leq 0, \tag{5.33}$$

where $\phi(x)$ represents the value of constraint violation at solution x and it can be calculated as follows.

$$\phi(x) = \sum_{j=1}^{q} (max\{0, g_j(x)\}) + \sum_{j=q+1}^{m} (max\{0, |h_j(x)|\}) \tag{5.34}$$

It is seen from Eqn. (5.33), a fixed value of ϵ is used to modify the feasible region for each constraint violation without considering the number of violated constraints. This ϵ value is shared among the violated constraints. Therefore, the infeasible region with a low number of violated constraints is getting more sharing of ϵ as compared to the infeasible region with a higher number of violated constraints. This may strongly degrade the performance on COPs with a higher number of constraints with the optimum solution at active constraints.

To demonstrate this issue, a pictorial representation of a simple COP having five linear constraints are shown in figure 5.3. It can be seen from figure 5.3 that the ϵ-level feasible region has a very low volume of relaxed feasible region nearer to the optimum value as compared to the volume of the relaxed feasible region of other areas. Since the main function of this relaxed feasible region is to facilitate the population to search solutions at the boundary of the feasible region then the very low volume of relaxed feasible region nearer to the optimum solution cannot be the best situation. In [195] and [196], relaxed equality and inequality constraint functions are used to create separate surrogate models for all constraints. Further, these surrogate models are utilized to generate new solutions for expansive COPs. The performance of these surrogate assisted algorithms is highly improved after using relaxed equality and inequality constraint functions in place of actual constraint functions [195].

To sum up, the separate relaxation of constraints can provide a sufficient volume of the relaxed feasible region, which is beneficial to explore the optimum solutions nearer to the boundaries of feasible regions. Nevertheless, this approach has been discovered in surrogate modeling but has not been utilized in constrained handling techniques by existing constrained optimizations EAs. To overcome the limitation of ϵ-level modification without losing its core properties and to utilize the features of separate relaxation of constraints, a υ-level modification is proposed in this study.

In υ-level modification, the boundaries of all the feasible regions are modified. It is done by subtracting υ from all the constraints of the problem as shown below:

$$g_i^{(\upsilon)}(x) \leq 0 \implies g_i(x) - \upsilon \leq 0, \tag{5.35}$$

where υ represents the υ-level and its value must be a non-negative number. Usually, there is no need to have υ-level modification in constraints and many problems can be solved where the value of υ-level is set to 0 during the optimization process. However, in case of problems with smaller feasible regions, a high number of active inequality and equality constraints, the υ-level modification in constraint with proper controlling of υ-level would be required to obtain the better quality solutions. The calculation and controlling procedure of υ-level is discussed in the later section.

It is worth noting here that the υ-level modification is applicable to inequality constraints only. As an equality constraint, $h_i(x) = 0$ can be replaced with two inequality

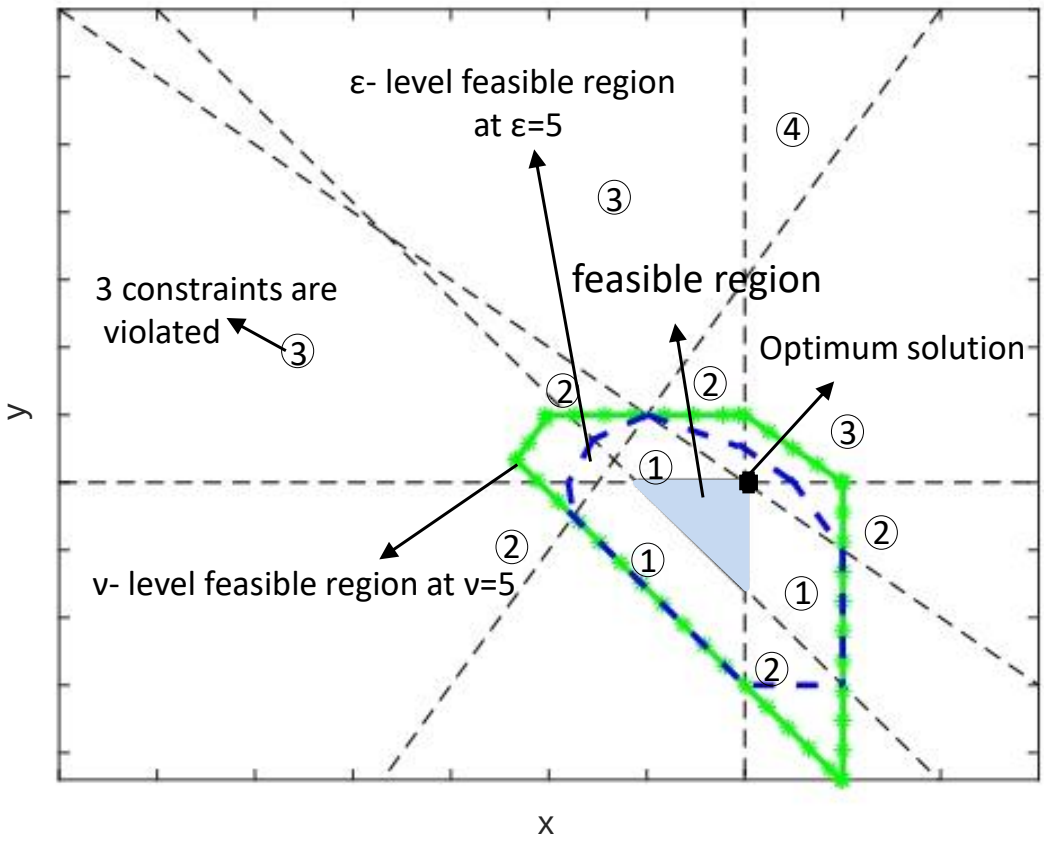

Figure 5.3: Graphical representation of main feature of υ-level modification as compared to ϵ-level comparison on a simple 2-D search space. Green solid line and blue dotted line represent the boundaries of υ-level and ϵ-level feasible regions respectively, at $\epsilon = \upsilon = 5$. Numbers within the circle represent the number of violated constraints in their respective area of search space.

constraints $h_i(x) \leq \epsilon_v$ and $-h_i(x) \leq \epsilon_v$, where ϵ_v is set to 10^{-4}. Thus, equality constraints can also be modified by υ-level modification as shown below.

$$|h_i^{(\upsilon)}(x)| \leq \epsilon_v \implies |h_i(x)| - \upsilon \leq \epsilon_v. \tag{5.36}$$

Moreover, we propose a simple procedure to control the υ-level at each iteration. The υ-level is only controlled for the first T iterations. After that, the υ-level is set to 0. The υ-level for each iteration is calculated as follows.

$$\upsilon_0 = \frac{\sum_{i=1}^{\theta\lambda} \phi_{i:\theta\lambda}}{\theta\lambda},$$

$$\upsilon^k = \begin{cases} \upsilon_0 \left(1 - \frac{k}{T}\right)^{\gamma} & , \ 0 < k \leq T, \\ 0 & , \ k > T, \end{cases} \tag{5.37}$$

where $\phi_{i:\theta N_p}$ represents the constraint violation of top i^{th} individual, $\theta = 0.9$, γ represents a parameter to control decay of the υ-level, and λ represents the population size. In this approach, it is presumed that the υ-level is equal to 10^{-5} (very small) at $k = 0.95T$. Now from Eqn. (5.37), this assumption can be reflected in the following way.

$$\upsilon^{0.95T} = \upsilon_0 \left(1 - \frac{0.95T}{T}\right)^{\gamma} = 10^{-5}. \tag{5.38}$$

Thus, parameter γ can be tuned according to Eqn. (5.38) and this can be done as shown below:

$$\gamma = max\left\{3, \frac{(-5 - log(\upsilon_0))}{log(0.05)}\right\}, \tag{5.39}$$

where the minimum value of γ is set to 3 to avoid too small a value for γ.

It is worth noting here that the value of T is problem dependent. The value of T can be fixed by using the sensitivity analysis over the wide variety of problems. From sensitivity analysis, it was found that the value of T can be set between 20% to 50% of the maximum allowed number of iterations.

Constraint violation and υ-level penalty function

In the υ-level penalty function, a υ-level constraint violation $\phi^{(\upsilon)}(x)$ is calculated by the sum of all the modified constraints:

$$\phi^{(\upsilon)}(x) = \sum_{j=1}^{q} (max\{0, g_j^{(\upsilon)}(x)\}) + \sum_{j=q+1}^{m} (max\{0, |h_j^{(\upsilon)}(x)| - \epsilon_v\}). \tag{5.40}$$

A v-level penalty function is defined as follows.

$$F(x) = f(x) + \alpha \cdot \phi^{(v)}(x), \tag{5.41}$$

where $f(x)$ and $F(x)$ denote the objective function value and fitness value at x respectively, and α is the penalty factor.

Calculation of the penalty factor α

Solving COPs with population-based EAs requires a balance between the minimization of the objective function and the constraint violation(s) during the optimization process. In [197], the correlation between constraint violation and objective function is calculated to guide the population for finding the feasible region. Although this approach performs well on COPs, a learning stage is required to calculate the correlation between the objective function and constrained violation. However, the correlation gained from the learning stage provides global correlation information and this correlation is not uniform over the search space. During the optimization process, it is more beneficial to use a local correlation between the objective function and constraints. In addition, no learning stage is required to calculate the local correlation between objective function and constraint which reduces the computational overhead. Here, we propose a simple approach to calculate the local correlation between the objective function and constraint violation to update the penalty factor.

Two kinds of relationship exist between constraints and the objective function.

1. The objective function $f(x)$ decreases as the degree of constraint violation $\phi^{(v)}(x)$ decreases.

2. The objective function $f(x)$ does not decreases as the degree of constraint violation $\phi^{(v)}(x)$ decreases.

For case (1), the objective function and constraint violation correlate with each other. In this situation, searching for a solution using constraint violation can easily stagnate the population in the feasible region. Therefore, the objective function value can help the solution to jump from the infeasible region to a feasible region. In such cases, the value of α should be equal to zero.

In the second type of relationship, objective function and constraint violation are not correlated to each other. Under this situation, too much weight to objective function or constraint violation may prevent the solution from stagnating the population. In such cases, the value of α should be tuned to provide proper weight to the objective function and constraint violation in fitness value.

To sum up, the value of α needs to tune according to the correlation between constraints and the objective function to guide the solutions to find the feasible region. However, this correlation information has not been utilized in the existing penalty functions. Hence a new self-adaptive technique is proposed in this chapter to auto-tune the value of α by using the correlation information.

At each iteration, the fitness value of the best solution should be lower than the fitness value of the other solution of the population of current or past iterations (in case of minimization problem). Mathematically, this relation can be represented in the following way:

$$f(y) + \alpha \cdot \phi^{(v)}(y) > f(x^*) + \alpha \cdot \phi^{(v)}(x^*), \tag{5.42}$$

where y represents a solution of population of the current or past generation and x^* represents the best solution found so far. Further, Eqn. (5.42) can be reduced to

$$\alpha > \frac{f(x^*) - f(y)}{\phi^{(v)}(y) - \phi^{(v)}(x^*)}. \tag{5.43}$$

The right hand side of Eqn. (5.43) indicate the relative variation of objective function value with respect to opposite variation of the constraint violation between the best solution and other solutions. When we mine this variation for all solutions of population, it provides the local correlation information between objective function and constraint in terms of relative variation from best solution.

In order to provide better mining of the correlation, an archive of solutions A_r of fixed size is formed which contains the solutions generated in past generations. When the size of this archive exceeds the fixed size, randomly selected solutions are discarded from the archive to maintain the size. From Eqn. (5.43),

$$\alpha^k > \frac{f(x^*) - f(y_i^k)}{\phi^{(v)}(y_i^k) - \phi^{(v)}(x^*)}, \tag{5.44}$$

where y_i^k represents the $i-$th individual of archive A_r and N_{A_r} represents the size of A_r. This information can be utilized to tune the value of penalty factor (α) in each iteration.

In v-level penalty function, we use the following equation to tune the value of α.

$$\alpha^k = max\left\{\frac{f(x^*) - f(y_i^k)}{\phi^{(v)}(y_i^k) - \phi^{(v)}(x^*)}, 0\right\}, \tag{5.45}$$

where $i = 1, 2, ...N_{A_r}$.

5.5.2 Broyden-based Mutation

In this subsection, Broyden-based Mutation is discussed.

Motivation

COPs with non-linear equality constraints can be hard to solve using COEAs. Most of constrained optimization EAs transform equality constraints into relaxed inequality constraints to solve these COPs. Feasible region of the search-space becomes very low due to the involvement of a large number of equality constraints. As a result, the performance of MA-ES (or CMA-ES) has been mediocre on these COPs as compared to other class of EAs. To address this issue, a gradient-based repair method is utilized in [1]. In literature, this repair method has also been utilized with other class of EAs such as in [198] with GA, and in [146] with DE. However, this repair method requires a large number of FEs (multiple of the number of decision variables) to repair a single infeasible solution. The main reason for the requirement of high function evaluations is the evaluation of gradient information (Jacobian matrix) of constraint space in each iteration of the repair process. In order to resolve this issue, a Broyden-based Mutation (BBM) technique is proposed in this chapter that requires only one FE in each iteration except for the first iteration to repair the infeasible solution. For the first iteration of the repairing process, the steps are similar to reported in [1].

Broyden's method

To solve a system of non-linear equations, $F(x) = [f_1(x), f_2(x)....f_n(x)]^T = 0$, where n is the total number of non-linear equations and $x = [x_1, x_2, \ldots .x_n]^T$, Newton's method is the computationaly inefficient due to the requirement of partial derivative of $F(x)$ at x (Jacobian matrix) during each iteration. This method cannot facilitate the reusing of information gained from previous iterations and in some situations determination of

the partial derivatives can be very costly. Finite-difference based calculation of partial derivatives of $F(x)$ at x requires n function evaluations (FEs) per iteration.

To overcome this issue of Newton's method, approximate partial derivatives can be used alternatively, since it provides slightly slower convergence due to approximation but it improves the efficiency overall. A simple and robust way to approximate the partial derivatives is proposed by C. G. Broyden in his seminal work on finding the solution of system of non-linear simultaneous equations [199]. In [199], the following equations are proposed to solve the simultaneous equations.

$$x^{(k+1)} = x^{(k)} - B^{-1(k)}F(x^{(k)}), \tag{5.46}$$

where

$$B^{-1(k)} = B^{-1(k-1)} + \frac{(s^{(k)} - B^{-1(k-1)}y^{(k)})(s^{(k)})^T B^{-1(k)}}{(s^{(k)})^T B^{-1(k-1)}y^{(k)}}, \tag{5.47}$$

$$s^{(k)} = x^{(k)} - x^{(k-1)}, \text{ and} \tag{5.48}$$

$$y^{(k)} = F(x^{(k)}) - F(x^{(k-1)}). \tag{5.49}$$

It can be seen from the above equations that an approximation of the inverse of the matrix of partial derivatives requires only one FE.

Proposed Scheme

Our proposed BBM to repair the infeasible solution is inspired by Broyden's method. The main steps of BBM are as follows:

1. First of all, all the constraints (Inequality, equality and bound constraints) of the COP are transformed into a system of simultaneous equations using slack variables, i.e.

$$g_j(x) + s_j^2 = 0, \ j = 1, ..., q, \tag{5.50}$$

$$h_j(x) = 0, \ j = q+1, ..., m, \tag{5.51}$$

$$x_i - l_i - lb_i^2 = 0, \ i = 1, ..., n, \tag{5.52}$$

$$x_i - u_i + ub_i^2 = 0, \ i = 1, ..., n, \tag{5.53}$$

   where, s_j, lb_i, and ub_i are the slack variables used to transform inequality, lower-bound, and upper-bound constraints into non-linear equations.

2. In second step, above mentioned system of simultaneous equations is solved using BBM (shown in Algorithm 4).

Algorithm 4: BBM(x)

Result: x, FE

Set $Max_{FE} \leftarrow (3D+1)$, and $TolF \leftarrow 10^{-15}$;

Define $s_j \leftarrow 0,\ j = 1, ..., q$, $lb_i \leftarrow \sqrt{x_i - l_i},\ , i = 1, ..., D$, and $ub_i \leftarrow \sqrt{u_i - x_i},\ , i = 1, ..., D$;

Initialize $\hat{x}^{(0)} \leftarrow [x^T, s_1, ..s_q, lb_1, ..lb_D, ub_1, ..ub_D]^T$;

$J \leftarrow$ Calculate Jacobian using Finite-difference approximation;

$FE \leftarrow D$;

$B^{-1(0)} \leftarrow$ PsuedoInverse(J);

$F^{(0)} \leftarrow F(\hat{x}^{(0)})$;

$FEs \leftarrow FEs + 1$;

$k \leftarrow 0$;

while $(FEs < Max_{FE})||(\|F^{(k)}\| > TolF)$ **do**

  $k \leftarrow k + 1$;

  $\hat{x}^{(k+1)} \leftarrow \hat{x}^{(k)} - B^{-1(k)}F^{(k)}$;

  $F^{(k+1)} \leftarrow F(\hat{x}^{(k+1)})$;

  $FE \leftarrow FE + 1$;

  $s^{(k+1)} \leftarrow \hat{x}^{(k+1)} - \hat{x}^{(k)}$;

  $y^{(k+1)} \leftarrow F^{(k+1)-F^{(k)}}$;

  $B^{-1(k+1)} \leftarrow B^{-1(k)} + \frac{(s^{(k+1)} - B^{-1(k)}y^{(k+1)})(s^{(k+1)})^T B^{-1(k)}}{(s^{(k+1)})^T B^{-1(k)} y^{(k+1)}}$;

end

$x \leftarrow \hat{x}^{(k)}_{1:D}$;

5.5.3 Proposed Algorithm: υMA-ESbm

The proposed algorithm, named υMA-ESbm, is described. MA-ES [200] is used as the core optimizer. In order to deal with the constraints of the problem, υ-level penalty function based constraint handling technique with Broyden-based mutation is consolidated in the framework of MA-ES described in [200]. The pseudo code of υMA-ESbm is shown in Algorithm 5.

Algorithm 5: υMA-ESbm

Result: $bestx$, $bestf$, and $bestc$

1 Set λ, μ, σ^0, σ_{max}, T, k_r, and θ_r;
2 Initialize the parameters of MA-ES at their default values as shown in Table 5.1;
3 Initialize $M^0 \leftarrow I$, $P_c \leftarrow 0$, and $X^0 \leftarrow \{x_1^0, x_2^0 .... x_\lambda^0\}$;
4 Evaluate f^0, g^0, and h^0 at each individual of X^0;
5 $FEs \leftarrow \lambda$;
6 $\phi_i^{(0)} \leftarrow \sum_j \max(g_{i,j}^0, 0) + \sum_j \max(|h_{i,j}^0| - e_v, 0)$, $i \in \{1, 2..\lambda\}$;
7 Calculate υ_0, γ, $\phi^{(\upsilon_0)}$, and α^0 using Eqns. (5.37), (5.39), (5.40), and (5.45) respectively ;
8 $F^0 \leftarrow f^0 + \alpha^0 \cdot \phi^{(\upsilon_0)}$;
9 $x_m^0 \leftarrow \sum_{i=1}^{\mu} w_i x_{i:\lambda}$ according to F^0;
10 $bestx \leftarrow x_{1:\lambda}^0$, and $bestf \leftarrow f_{1:\lambda}^0$;
11 $bestc \leftarrow \sum_j \max(g_{1:\lambda}^0, 0) + \sum_j \max(|h_{1:\lambda}^0| - e_v, 0)$;
12 $k \leftarrow 0$;
13 **while** $FEs \leq FE_{max}$ **do**
14 $k \leftarrow k + 1$;
15 $M^{-1} \leftarrow \text{PseudoInverse}(M^k)$;
16 **for** $i \leftarrow 1 : \lambda$ **do**
17 $z_i^k \leftarrow N(0, I)$, $d_i^k \leftarrow M^k z_i^k$ and $\bar{x} \leftarrow x_i^k + \sigma^k d_i^k$;
18 $x_i^{k+1} \leftarrow \text{KeepRange}(\bar{x})$;
19 Evaluate f_i, g_i, and h_i at x_i^{k+1};
20 $FEs \leftarrow FEs + 1$;
21 Calculate $\phi_i^{(\upsilon)}$ using Eqn. (5.40);
22 **if** $(mod(k, D) == 0) || (U(0,1) < \theta_r)$ **then**
23 $[x_i^{k+1}, FE] \leftarrow \text{BBM}(x_i^{k+1})$;
24 $FEs \leftarrow FEs + FE$
25 **end**
26 **if** $\bar{x} \neq x_i^{k+1}$ **then**
27 $d_i^k \leftarrow \frac{x_i^{k+1} - \bar{x}}{\sigma^k}$, $z_i^k \leftarrow M^{-1} d_i^k$;
28 Calculate $\phi_i^{(\upsilon)}$ using Eqn. (5.40);
29 **end**
30 **end**
31 Calculate α using Eqn. (5.45);
32 $F^k \leftarrow f^k + \alpha^k \cdot \phi^{(\upsilon^k)}$;
33 $x_m^{k+1} \leftarrow x_m^k + \sigma^k \sum_{i=1}^{\mu} w_i d_{1:\lambda}^k$ according to F;
34 Update P_c^{k+1}, M^{k+1}, σ^{k+1}, and υ^{k+1} using Eqns. (5.56), (6.48), (5.58), and (5.37);
35 Update $bestx$, $bestf$, and $bestc$ using Deb's rule [201];
36 **end**

The main steps of υMA-ESbm are described as follows.

- **Step 1** (Line 1-3): Firstly, parameters of algorithm are set to their default values and an initial population X^0 of λ solutions are randomly generated within the bounds of the search space using following equation.

$$x_{i,j}^0 = l_j + (u_j - l_j) \cdot \text{U}(0,1), \ \ for\ i = 1, 2.....\lambda, \tag{5.54}$$

Table 5.1: Default value of parameters of MA-ES [1]

1.	$w_i = \frac{ln(\mu+0.5)-ln(i)}{\sum_{j=1}^{\mu}(ln(\mu+0.5)-ln(j))},\ for\ i \in \{1,..,\mu\},$	
2.	$\mu_{eff} = \frac{1}{\sum_{i=1}^{\mu} w_i^2},$	3. $c = \frac{\mu_{eff}+2}{D+\mu_{eff}+5},$
4.	$c_p = \frac{2}{(D+1.3)^2+\mu_{eff}},$	5. $c_z = min\left[1-c_p, \frac{2(\mu_{eff}-2+1/\mu_{eff})}{(D+1)^2+\mu_{eff}}\right].$

where, $x_{i,j}$ represents $j-$th element of x_i^0 and $\mathrm{U}(0,1)$ a uniformly distributed random number in $(0,1)$.

- **Step 2** (Line 4-12): The initial population is used to determine the υ_0 and γ. Then, the initial recombinant, x_m^0, is obtained using weighted recombination of the top μ individuals of population X^0.

- **Step 3** (Line 17-21): By using σ^k and M^k, new solutions are generated for each λ solutions in the mutation operation. If a new solution is sampled outside the bounds of the search space, then that solution is reflected back to search space using Eqn. (5.55) (Line 18, KeepRange function).

$$x_{i,j} = \begin{cases} 2 \times l_j - x_{i,j} - \left\lfloor \frac{l_j - x_{i,j}}{v_i} \right\rfloor v_i, & if \mathrm{x\dot{}i,j\ ¡\ l\dot{}j} \\ x_{i,j} - \left\lfloor \frac{x_{i,j}-v_j}{v_i} \right\rfloor_i, & if \mathrm{x\dot{}i,j¿u\dot{}j} \\ x_{i,j} & else \end{cases} \tag{5.55}$$

where $v_i = (l_j - u_j)$.

- **Step 4** (Line 22-25): If the iteration count, k, becomes multiple of dimension D, BBM operator is used with probability θ_r to generate the feasible solutions to replace the infeasible ones.

- **Step 5** (Line 26-29): The corresponding vectors d_i^k and z_i^k of the readjusted x_i^k are recalculated to the correct value. Inverse of M^k is required for this process.

- **Step 6** (Line 31-34): Calculates the penalty factor α by using Eqn. (5.45). Vector P_c^{k+1} is updated using Eqn. (5.56) and matrix M^{k+1} is updated using P_c^{k+1}, M^k, z^k as shown in Eqn (6.48), and other parameters. Finally, the mutation step-size σ^{k+1} is updated using the value of P_c^{k+1} as shown in Eqn. (5.58).

$$P_c^{k+1} = (1-c)P_c^k + \sqrt{c(2-c)\mu_{eff}} \sum_{i=1}^{\mu} w_i z_{i:\lambda}^k, \tag{5.56}$$

$$M^{k+1} = M^k + \frac{c_p}{2} M^k (P_c^{k+1}(P_c^{k+1})^T - I)...$$
$$+ \frac{c_z}{2} M^k \left(\sum_{i=1}^{\mu} w_i z_{i:\lambda}^k (z_{i:\lambda}^k)^T - I \right), \tag{5.57}$$

$$\sigma^{k+1} = min \left(\sigma^k exp \left[\frac{c}{2} \left(\frac{||P_c^{k+1}||^2}{D} - 1 \right) \right], \sigma_{max} \right), \tag{5.58}$$

where c, c_p, and c_z are learning rate parameters of MA-ES which are set to their default values.

- **Step 7** (Line 35): Best solution with its objective function and constraint violation value are updated using Deb's rule [201] of selection of solution.
- **Step 8** (Line 15): If the inverse of M is ill-conditioned then M is reinitialized to Identity matrix.
- **Step 9** (Line 13): Go to **Step 3**, if the FEs is less than the maximum allowed number of function evaluation.
- **Step 10** (Line 36): Return the best solution with its objective function and constraint violation value.

The performance of υMAESlm has been validated on benchmark problems and reported in Appendix-III.

5.6 Performance of Proposed Algorithm

Two novel algorithms, ϵDE-GN, and υMAESbm, have been implemented to optimize the objective function corresponding to power flow problem. ϵDE-GN algorithm uses DE as a search algorithm with a Gauss-Newton mutation operator. υMAESbm uses MAES as a search algorithm with Broyden mutation operator.

To analyze the accuracy of the obtained results from the proposed algorithms, a comparison of voltages obtained from the proposed algorithms and PSCAD/EMTDC is performed on the 6-bus system. The results obtained from PSCAD, ϵDE-GN, and υMAESbm are depicted in Table-5.2. It is clearly seen from Table-5.2 that the maximum errors in voltage magnitude and angle are 0.0081% and 0.26% respectively. This good agreement within the obtained results validates the accuracy of the ϵDE-GN, and

Table 5.2: Validation of obtained result of the six-bus test system

Bus	Voltage magnitude (V)			Angle (rad)		
	PSCAD	ϵDE-GN	υMAESbm	PSCAD	ϵDE-GN	υMAESbm
1	121.92	121.92	121.92	0.0078	0.0078	0.0078
2	123.51	123.51	123.51	-0.0013	-0.0013	-0.0013
3	122.42	122.42	122.42	-0.0388	-0.0389	-0.0389
4	125.37	125.37	125.37	0.0065	0.0065	0.0065
5	125.74	125.74	125.74	0*	0*	0*
6	123.11	123.10	123.10	-0.0420	-0.0421	-0.0426
err		0.0081%	0.0081%		0.26%	0.26%
freq	376.6645	376.6645	376.6645			
Time	172s	0.4s	0.9s			

Table 5.3: Comparison of results on 33-bus system

Methods	Mean	Stdev	CT
GA	1.48×10^{-04}	1.02×10^{-04}	4.3s
PSO	2.04×10^{-06}	1.83×10^{-06}	2.2s
Newton-trust	1.73×10^{-06}	1.07×10^{-06}	1.7s
ϵDE-GN	1.58×10^{-09}	1.43×10^{-09}	0.8s
υMAESbm	1.25×10^{-10}	1.08×10^{-10}	1.1s

υMAESbm in solving the power flow of droop control based islanded MG. Moreover, PSCAD requires approximately 172s to attain the steady-state, while the ϵDE-GN, and υMAESbm require 0.4s and 0.9s respectively.

Further, a comparison among different optimization algorithms, GA, PSO, Newton-trust region, ϵDE-GN, and υMAESbm has also been done for a 33-bus test system. The values of the means and standard deviations of the objective function with computation time are depicted for each of the algorithms in Table 5.3. This Table shows that the proposed algorithms outperform the other contenders in terms of accuracy and computation time.

5.7 Case Studies

In this section, four case studies were carried out to validate the load flow flow algorithms on different test systems. The framework of these cases studies are as follows:

- **Case study I**: In this case, CASE6 test system was adopted to validate the proposed load flow algorithms. Fig. 5.4 shows topology of CASE6 test system as an islanded microgrid. The load data and line connectivity data used in test systems are reported in Appendix-II. This system consist of three similar droop controlled DGs on buses 4, 5 and 6 and the system is operated in islanded mode. The detailed specifications of droop controls are depicted in Table. 5.4. The effectuation of the proposed load flow algorithms as well as a comparative analysis using PSCAD software [40], the PSO method [23] are depicted in Table 5.4. Following are the observations:

  1. The steady state frequency obtained by proposed algorithms are 0.99924 p.u.
  2. The comparative analysis of the maximum magnitude and maximum phase errors of above specified methods against the proposed methods are 0.0008 and 0.007, respectively .

  Based on the above comparative analysis, it can be concluded that the proposed algorithms perform with acceptable accuracy on droop controlled microgrids in islanded mode of operation.

Table 5.4: Droop control settings of DGs in CASE6 test system [56]

DG	Location	m_p	n_q	ω^*	V^*	S_{max}	Q_{max}
1	4	1.1439×10^{-3}	0.0591	1	1.01	1	0.7
2	5	1.1439×10^{-3}	0.0591	1	1.01	1	0.7
3	6	1.1439×10^{-3}	0.0591	1	1.01	1	0.7

- **Case study II:** The IEEE CASE69 distribution system shown in Fig.5.5 has been considered for this case study as an islanded microgrid. This system is having total active and reactive loads of 3.772 MW and 2.694 MVAr respectively. Bus numbers 50, 27, 35, 46 and 65 are considered for DGs installation. The detailed droop control setting of DGs for the CASE69 distribution system reported in Table 5.6 are adopted

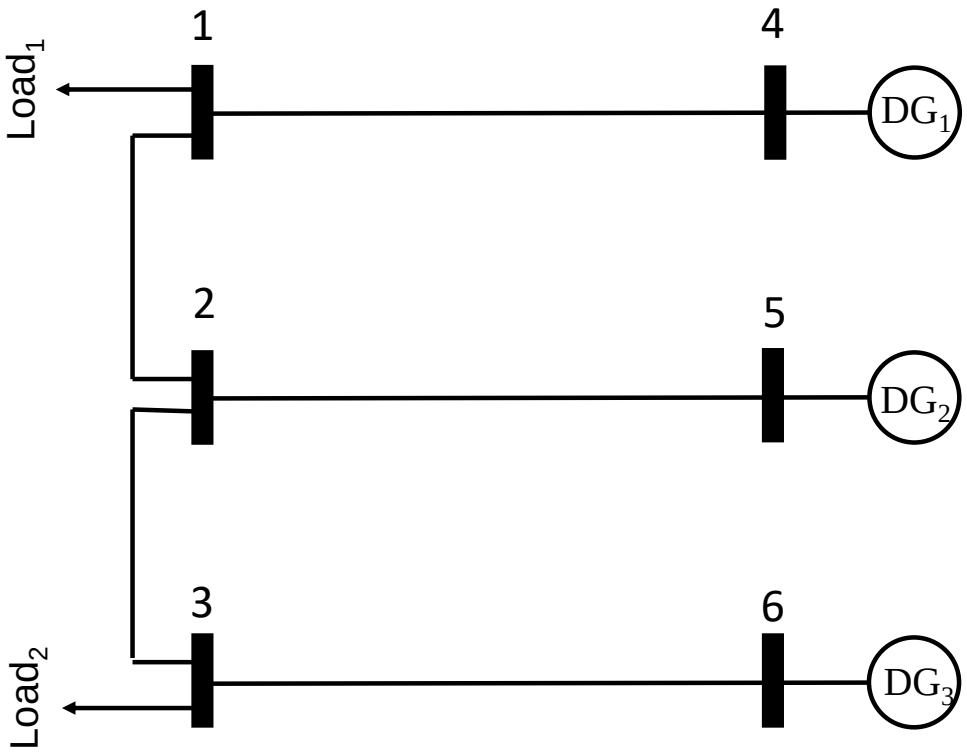

Figure 5.4: Topology of CASE6 test system operated as an islanded microgrid.

Table 5.5: Outcomes of proposed load flow algorithm for a CASE6 test system compared with other methods.

Bus	Time domain Model		ϵDE-GN		υMAESbm		PSO		Newton-trust	
	$\|V\|$	$\angle_V$	$\|V\|$	$\angle_V$	$\|V\|$	$\angle_V$	$\|V\|$	$\angle_V$	$\|V\|$	$\angle_V$
1	0.9605	0	0.9606	0	0.9606	0	0.9607	0	0.9601	0
2	0.9730	-0.537	0.9729	-0.5291	0.9730	-0.5269	0.9728	-0.5292	0.9725	-0.5262
3	0.9643	-2.685	0.9647	-2.6837	0.9646	-2.6828	0.9645	2.6765	0.9638	-2.6822
4	0.9877	-0.0725	0.9875	-0.0726	0.9877	-0.0716	0.9884	-0.0727	0.9873	-0.0722
5	0.9906	-0.452	0.9903	-0.4516	0.9905	-0.4522	0.9883	-0.0454	0.9901	-0.45101
6	0.9698	-2.869	0.9689	-2.8668	0.9698	-2.8659	0.9701	-2.8608	0.9694	-2.8653

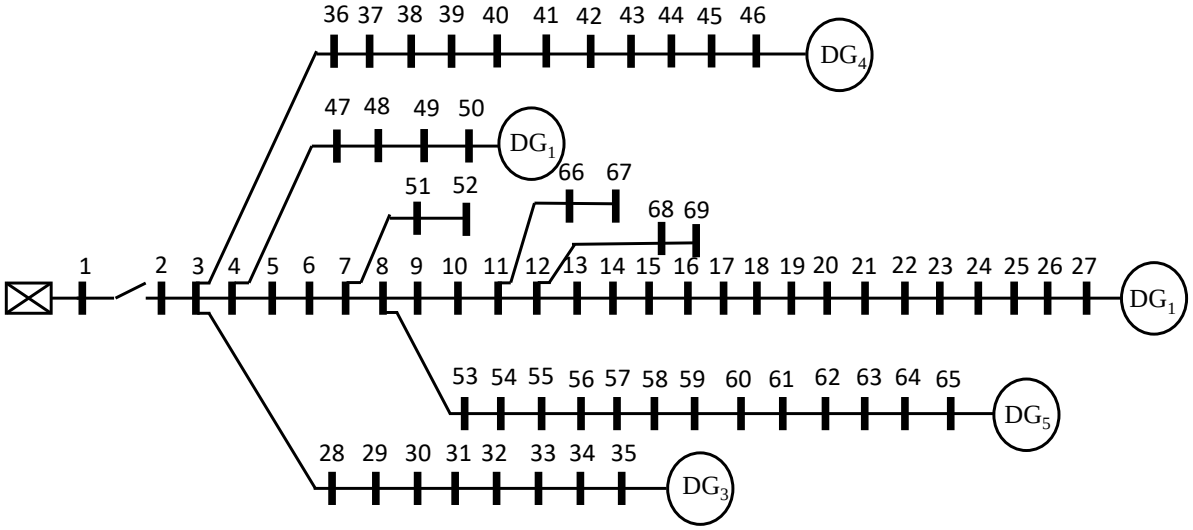

Figure 5.5: Topology of CASE69 test system operated as an islanded microgrid.

for analyses purpose. Tables 5.7 and 5.8 present the detailed voltage profile obtained using ϵDE-GN and υMAESbm, respectively. Following are the observations.

1. The steady state frequency obtained by ϵDE-GN and υMAESbm are 0.9977 p.u and 0.9977 p.u., respectively.
2. The total active power and reactive power load demand on the distribution system are 3.7722 MW and 2.6941 MVAr respectively whereas active and reactive power losses are 0.0868 MW and 0.0424 MVAR.

- **Case study III:** A CASE33 distribution system with bus voltage of 12.66 kV is used in this case study for demonstration of proposed load flow algorithm. The single

Table 5.6: Droop control settings of DGs in CASE69 test system [2]

DG	Location	m_p	n_q	ω^*	V^*	S_{max}	Q_{max}
1	60	1.501×10^{-3}	0.03333	1	1.04	2.0	1.4
2	27	4.504×10^{-3}	0.01	1	1.04	1.0	0.65
3	35	2.308×10^{-3}	0.05	1	1.04	1.2	0.6
4	46	2.308×10^{-3}	0.05	1	1.04	1	0.6
5	65	1.501×10^{-3}	0.03333	1	1.04	1.5	0.9

Table 5.7: Voltage profile obtained from ϵDE-GN for CASE69 distribution system operated as an islanded microgrid.

Bus	$\lvert V\rvert$	$\angle_V$	P	Q	$\lvert I\rvert$	$\angle_I$	Bus	$\lvert V\rvert$	$\angle_V$	P	Q	$\lvert I\rvert$	$\angle_I$	Bus	$\lvert V\rvert$	$\angle_V$	P	Q	$\lvert I\rvert$	$\angle_I$
1	–	–	–	–	–	–	24	0.9711	-0.1277	-0.0280	-0.0200	0.0208	2.2516	47	0.9712	-0.0001	0.0000	0.0000	0.0061	-0.7545
2	0.9710	0.0000	0.0000	0.0000	0.0033	-0.5378	25	0.9870	-0.1356	0.0000	0.0000	0.0032	0.5156	48	0.9730	0.0039	-0.0790	-0.0564	0.0592	2.5486
3	0.9710	0.0000	0.0000	0.0000	0.0063	-0.8331	26	0.9936	-0.1388	-0.0140	-0.0100	0.0105	2.2647	49	0.9815	0.0190	-0.3847	-0.2745	0.2893	2.5477
4	0.9712	-0.0003	0.0000	0.0000	0.0057	-0.8002	27	0.9974	-0.1407	0.4940	0.6374	0.3698	-0.9093	50	0.9872	0.0254	-0.3847	-0.2745	0.6281	-0.3321
5	0.9711	-0.0037	0.0000	0.0000	0.0150	-0.9815	28	0.9706	0.0005	-0.0260	-0.0186	0.0275	2.5083	51	0.9401	-0.0825	-0.0405	-0.0283	0.0292	2.4537
6	0.9571	-0.0377	-0.0026	-0.0022	0.0225	-1.2498	29	0.9648	0.0073	-0.0260	-0.0186	0.0234	2.3300	52	0.9400	-0.0825	-0.0036	-0.0027	0.0029	2.4250
7	0.9433	-0.0737	-0.0404	-0.0300	0.0183	2.8487	30	0.9688	0.0293	0.0000	0.0000	0.0050	-0.6933	53	0.9373	-0.1039	-0.0043	-0.0035	0.0068	-0.8428
8	0.9403	-0.0826	-0.0750	-0.0540	0.0612	2.4732	31	0.9695	0.0332	0.0000	0.0000	0.0047	-0.7149	54	0.9356	-0.1232	-0.0264	-0.0190	0.0095	2.4035
9	0.9390	-0.0874	-0.0300	-0.0220	0.0128	2.4806	32	0.9732	0.0526	0.0000	0.0000	0.0130	-0.6912	55	0.9340	-0.1504	-0.0240	-0.0172	2.1961	-1.3162
10	0.9279	-0.0876	-0.0280	-0.0190	0.0189	2.5090	33	0.9828	0.0986	-0.0140	-0.0100	0.0178	-0.7815	56	0.8995	-0.1475	0.0000	0.0000	0.0503	1.0580
11	0.9256	-0.0877	-0.1450	-0.1040	0.1145	2.4455	34	1.0074	0.1901	-0.0195	-0.0140	0.0215	-0.8037	57	0.7209	-0.0983	0.0000	0.0000	0.0691	1.0531
12	0.9231	-0.0901	-0.1450	-0.1040	0.1109	2.4370	35	1.0335	0.2664	1.0099	-0.9140	0.8479	1.1568	58	0.6334	-0.0694	0.0000	0.0000	0.0415	1.1028
13	0.9295	-0.0969	-0.0080	-0.0055	0.0041	2.1597	36	0.9710	0.0003	-0.0260	-0.0186	0.0275	2.5237	59	0.5996	-0.0571	-0.1000	-0.0720	0.1140	2.2052
14	0.9362	-0.1038	-0.0080	-0.0055	0.0043	2.1304	37	0.9715	0.0051	-0.0260	-0.0186	0.0212	2.5374	60	0.5598	-0.0405	0.4486	1.3111	0.0548	-1.5506
15	0.9434	-0.1109	0.0000	0.0000	0.0018	-0.2209	38	0.9736	0.0094	0.0000	0.0000	0.0038	-0.8084	61	0.5012	-0.0292	-1.2440	-0.8880	1.3428	2.5328
16	0.9447	-0.1122	-0.0455	-0.0300	0.0338	2.4396	39	0.9741	0.0106	-0.0240	-0.0170	0.0187	2.6245	62	0.4991	-0.0287	-0.0320	-0.0230	0.0022	1.2631
17	0.9480	-0.1150	-0.0600	-0.0350	0.0429	2.4945	40	0.9742	0.0107	-0.0240	-0.0170	0.0185	2.6275	63	0.4959	-0.0281	0.0000	0.0000	0.0073	2.4883
18	0.9481	-0.1150	-0.0600	-0.0350	0.0431	2.4941	41	0.9911	0.0405	-0.0012	-0.0010	0.0051	-1.8529	64	0.4807	-0.0251	-0.2270	-0.1620	0.2435	2.5459
19	0.9528	-0.1178	0.0000	0.0000	0.0011	0.2747	42	0.9985	0.0531	0.0000	0.0000	0.0018	-1.5648	65	0.4761	-0.0242	1.4649	0.0565	0.0633	2.5506
20	0.9558	-0.1196	-0.0010	-0.0006	0.0010	0.2978	43	0.9995	0.0547	-0.0060	-0.0043	0.0058	2.6485	66	0.9252	-0.0875	-0.0180	-0.0130	0.0130	2.4392
21	0.9607	-0.1224	-0.1140	-0.0810	0.1141	2.3989	44	0.9997	0.0551	0.0000	0.0000	0.0019	-0.9064	67	0.9252	-0.0875	-0.0180	-0.0130	0.0138	2.4378
22	0.9610	-0.1226	-0.0053	-0.0035	0.0239	-0.7357	45	1.0023	0.0598	-0.0392	-0.0263	0.0442	2.8316	68	0.9210	-0.0894	-0.0280	-0.0200	0.0216	2.4428
23	0.9642	-0.1242	0.0000	0.0000	0.0013	0.7907	46	1.0023	0.0598	0.9767	0.1198	0.5296	0.1773	69	0.9210	-0.0894	-0.0280	-0.0200	0.0218	2.4425
w	0.9977																			

line diagram of distribution system shown in Fig. 5.6 with four DGs on bus number 26, 22, 25 and 9 and this test system is operated in islanded mode. The static droop coefficient of DGs along with relevant specification are depicted in Table. 5.9. The coefficients k_{pf} and k_{qf} (equations 5.3 and 5.4) for all DGs were assumed as 1 and -1 respectively. In this case, analysis have been performed assuming DG1 operates in PV mode, whereas other DGs are operating in droop controlled mode. Often constant power load modeling is taken into load flow formulation, whereas in this work loads are modeled to mimic real scenario in form of commercial, residential and industrial load models which were obtained by using equations 5.3 and 5.4. The

Table 5.8: Voltage profile obtained from υMAESbm for CASE69 distribution system operated as an islanded microgrid.

Bus	$\|V\|$	$\angle_V$	P	Q	$\|I\|$	$\angle_I$	Bus	$\|V\|$	$\angle_V$	P	Q	$\|I\|$	$\angle_I$	Bus	$\|V\|$	$\angle_V$	P	Q	$\|I\|$	$\angle_I$
1	–	–	–	–	–	–	24	0.9711	-0.1277	-0.0280	-0.0200	0.0208	2.2516	47	0.9712	-0.0001	0.0000	0.0000	0.0061	-0.7545
2	0.9710	0.0000	0.0000	0.0000	0.0033	-0.5378	25	0.9870	-0.1356	0.0000	0.0000	0.0032	0.5156	48	0.9730	0.0039	-0.0790	-0.0564	0.0592	2.5486
3	0.9710	0.0000	0.0000	0.0000	0.0063	-0.8331	26	0.9936	-0.1388	-0.0140	-0.0100	0.0105	2.2647	49	0.9815	0.0190	-0.3847	-0.2745	0.2893	2.5477
4	0.9712	-0.0003	0.0000	0.0000	0.0057	-0.8002	27	0.9974	-0.1407	0.4940	0.6374	0.3698	-0.9093	50	0.9872	0.0254	-0.3847	-0.2745	0.6281	-0.3321
5	0.9711	-0.0037	0.0000	0.0000	0.0150	-0.9815	28	0.9706	0.0005	-0.0260	-0.0186	0.0275	2.5083	51	0.9401	-0.0825	-0.0405	-0.0283	0.0292	2.4537
6	0.9571	-0.0377	-0.0026	-0.0022	0.0225	-1.2498	29	0.9648	0.0073	-0.0260	-0.0186	0.0234	2.3300	52	0.9400	-0.0825	-0.0036	-0.0027	0.0029	2.4250
7	0.9433	-0.0737	-0.0404	-0.0300	0.0183	2.8487	30	0.9688	0.0293	0.0000	0.0000	0.0050	-0.6933	53	0.9373	-0.1039	-0.0043	-0.0035	0.0068	-0.8428
8	0.9403	-0.0826	-0.0750	-0.0540	0.0612	2.4732	31	0.9695	0.0332	0.0000	0.0000	0.0047	-0.7149	54	0.9356	-0.1232	-0.0264	-0.0190	0.0095	2.4035
9	0.9390	-0.0874	-0.0300	-0.0220	0.0128	2.4806	32	0.9732	0.0526	0.0000	0.0000	0.0130	-0.6912	55	0.9340	-0.1504	-0.0240	-0.0172	2.1961	-1.3162
10	0.9279	-0.0876	-0.0280	-0.0190	0.0189	2.5090	33	0.9828	0.0986	-0.0140	-0.0100	0.0178	-0.7815	56	0.8995	-0.1475	0.0000	0.0000	0.0503	1.0580
11	0.9256	-0.0877	-0.1450	-0.1040	0.1145	2.4455	34	1.0074	0.1901	-0.0195	-0.0140	0.0215	-0.8037	57	0.7209	-0.0983	0.0000	0.0000	0.0691	1.0531
12	0.9231	-0.0901	-0.1450	-0.1040	0.1109	2.4370	35	1.0335	0.2664	1.0099	-0.9140	0.8479	1.1568	58	0.6334	-0.0694	0.0000	0.0000	0.0415	1.1028
13	0.9295	-0.0969	-0.0080	-0.0055	0.0041	2.1597	36	0.9710	0.0003	-0.0260	-0.0186	0.0275	2.5237	59	0.5996	-0.0571	-0.1000	-0.0720	0.1140	2.2052
14	0.9362	-0.1038	-0.0080	-0.0055	0.0043	2.1304	37	0.9715	0.0051	-0.0260	-0.0186	0.0212	2.5374	60	0.5598	-0.0405	0.4486	1.3111	0.0548	-1.5506
15	0.9434	-0.1109	0.0000	0.0000	0.0018	-0.2209	38	0.9736	0.0094	0.0000	0.0000	0.0038	-0.8084	61	0.5012	-0.0292	-1.2440	-0.8880	1.3428	2.5328
16	0.9447	-0.1122	-0.0455	-0.0300	0.0338	2.4396	39	0.9741	0.0106	-0.0240	-0.0170	0.0187	2.6245	62	0.4991	-0.0287	-0.0320	-0.0230	0.0022	1.2631
17	0.9480	-0.1150	-0.0600	-0.0350	0.0429	2.4945	40	0.9742	0.0107	-0.0240	-0.0170	0.0185	2.6275	63	0.4959	-0.0281	0.0000	0.0000	0.0073	2.4883
18	0.9481	-0.1150	-0.0600	-0.0350	0.0431	2.4941	41	0.9911	0.0405	-0.0012	-0.0010	0.0051	-1.8529	64	0.4807	-0.0251	-0.2270	-0.1620	0.2435	2.5459
19	0.9528	-0.1178	0.0000	0.0000	0.0011	0.2747	42	0.9985	0.0531	0.0000	0.0000	0.0018	-1.5648	65	0.4761	-0.0242	1.4649	0.0565	0.0633	2.5506
20	0.9558	-0.1196	-0.0010	-0.0006	0.0010	0.2978	43	0.9995	0.0547	-0.0060	-0.0043	0.0058	2.6485	66	0.9252	-0.0875	-0.0180	-0.0130	0.0130	2.4392
21	0.9607	-0.1224	-0.1140	-0.0810	0.1141	2.3989	44	0.9997	0.0551	0.0000	0.0000	0.0019	-0.9064	67	0.9252	-0.0875	-0.0180	-0.0130	0.0138	2.4378
22	0.9610	-0.1226	-0.0053	-0.0035	0.0239	-0.7357	45	1.0023	0.0598	-0.0392	-0.0263	0.0442	2.8316	68	0.9210	-0.0894	-0.0280	-0.0200	0.0216	2.4428
23	0.9642	-0.1242	0.0000	0.0000	0.0013	0.7907	46	1.0023	0.0598	0.9767	0.1198	0.5296	0.1773	69	0.9210	-0.0894	-0.0280	-0.0200	0.0218	2.4425
w	0.9977																			

load exponents for commercial, residential and industrial load are given in Table 5.10. Following are the observations:

1. The steady state frequency obtained by ϵDE-GN and υMAESbm for this case are 0.9984 p.u and 0.9984 p.u, respectively.
2. The detailed voltage and load profile of the CASE33 distribution system are presented in Table. 5.11.
3. Reactive power generation reaches maximum when the voltage of bus 22 equals 1.0075 p.u. whereas reactive power generation is fixed at its maximum value, when the voltage of bus 22 equals to 1.01 p.u. keeping the value of reactive power of droop controlled DGs within in their permissible range.

- **Case study IV:** The CASE25, a three phase unbalanced distribution operating in isolated mode, with the rated voltage of 12.66 KV has been adopted for this study. Fig. 5.7 shows typical topology of 25-bus distribution system as an islanded microgrid. The load data, line connectivity and impedances for different type of conductor used in distribution system are given in ref. [202]. Three DGs are installed

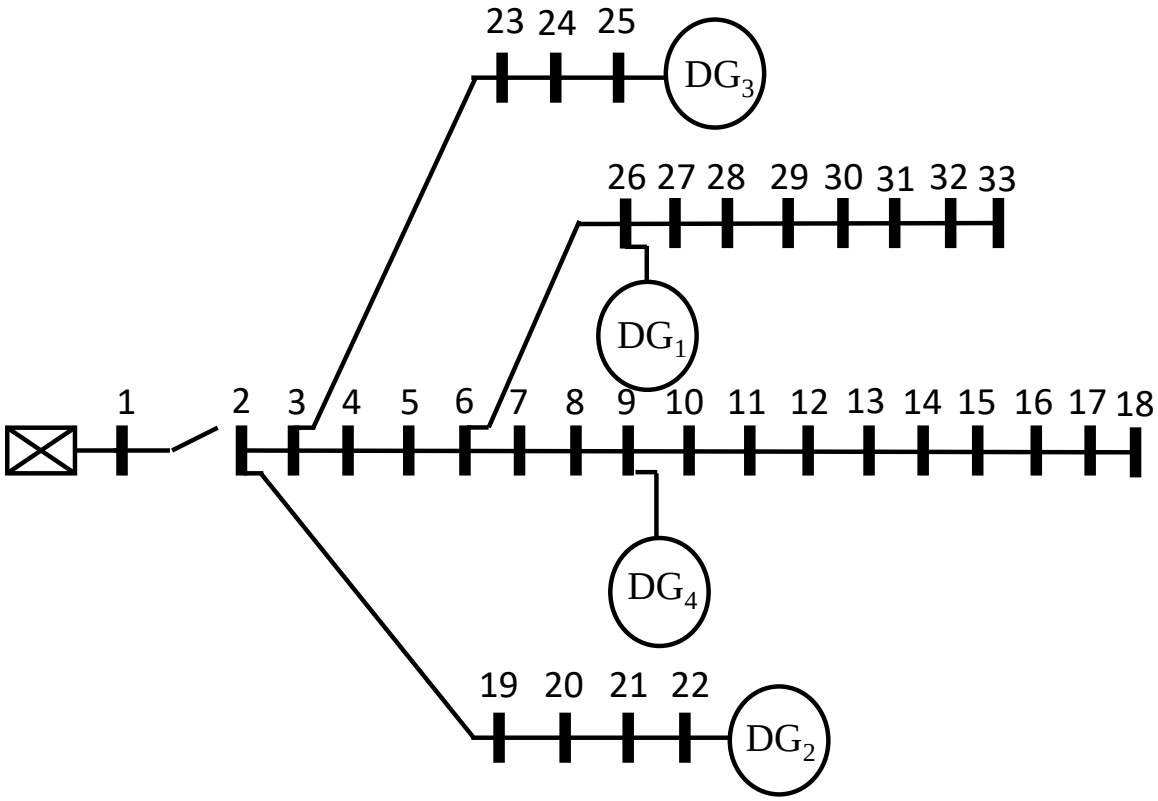

Figure 5.6: Topology of CASE33 system operating in islanded mode

Table 5.9: Droop control settings of DGs in CASE33 system [2]

DG	Location	m_p	n_q	ω^*	V^*	S_{max}	Q_{max}
1	26	0.705×10^{-3}	0.01667	1	1	3.5	1.8
2	22	2.252×10^{-3}	0.05	1	1	1.5	0.6
3	25	4.504×10^{-3}	0.01	1	1	1.5	1.3
4	9	3.003×10^{-3}	0.0667	1	1	1.5	1

Table 5.10: Load exponents of different loads

Load	α	β
constant	0	0
industrial	0.18	6
residential	0.92	4.04
commercial	1.51	3.4

Table 5.11: Voltage profile obtained by ϵDE-GN for CASE33 distribution system operated as an islanded microgrid.

Bus	$\lvert V\rvert$	$\angle_V$	P	Q	$\lvert I\rvert$	$\angle_I$	Bus	$\lvert V\rvert$	$\angle_V$	P	Q	$\lvert I\rvert$	$\angle_I$	Bus	$\lvert V\rvert$	$\angle_V$	P	Q	$\lvert I\rvert$	$\angle_I$
1	–	–	–	–	–	-	12	0.9830	0.0003	-0.1200	-0.0700	0.1413	2.6138	23	0.9906	-0.0015	-0.1800	-0.1000	0.2079	2.6330
2	0.9922	0.0000	-0.2000	-0.1200	0.2351	2.6012	13	0.9773	-0.0011	-0.1200	-0.0700	0.1422	2.6124	24	0.9908	-0.0043	-0.8400	-0.4000	0.9390	2.6929
3	0.9909	-0.0001	-0.1800	-0.0800	0.1988	2.7233	14	0.9752	-0.0023	-0.2400	-0.1600	0.2958	2.5513	25	0.9944	-0.0064	0.4205	1.0644	1.1509	-1.2010
4	0.9905	0.0009	-0.2400	-0.1600	0.2912	2.5545	15	0.9738	-0.0029	-0.1200	-0.0200	0.1249	2.9736	26	0.9912	0.0051	3.0831	1.3764	3.4062	-0.4148
5	0.9906	0.0018	-0.1200	-0.0600	0.1354	2.6798	16	0.9725	-0.0033	-0.1200	-0.0400	0.1301	2.8166	27	0.9888	0.0060	-0.1200	-0.0500	0.1315	2.7528
6	0.9906	0.0043	-0.1200	-0.0400	0.1277	2.8241	17	0.9706	-0.0044	-0.1200	-0.0400	0.1303	2.8154	28	0.9779	0.0073	-0.1200	-0.0400	0.1294	2.8271
7	0.9901	0.0029	-0.4000	-0.2000	0.4517	2.6808	18	0.9701	-0.0046	-0.1800	-0.0800	0.2031	2.7188	29	0.9701	0.0085	-0.2400	-0.1400	0.2864	2.6220
8	0.9896	0.0022	-0.4000	-0.2000	0.4519	2.6801	19	0.9928	0.0002	-0.1800	-0.0800	0.1984	2.7236	30	0.9667	0.0102	-0.4000	-1.2000	1.3085	1.9027
9	0.9907	0.0010	1.3207	0.9988	1.6713	-0.6465	20	1.0000	0.0024	-0.1800	-0.0800	0.1970	2.7258	31	0.9627	0.0089	-0.3000	-0.1400	0.3439	2.7138
10	0.9853	0.0000	-0.1200	-0.0400	0.1284	2.8199	21	1.0024	0.0036	-0.1800	-0.0800	0.1965	2.7269	32	0.9618	0.0085	-0.4200	-0.2000	0.4837	2.7057
11	0.9845	0.0001	-0.0900	-0.0600	0.1099	2.5537	22	1.01	0.0063	1.4410	0.6	1.5769	-0.4285	33	0.9616	0.0084	-0.1200	-0.0800	0.1500	2.5620
w	0.9984																			

at bus number 13, 19 and 25. The static droop coefficient of DGs along with relevant specification are depicted in Table. 5.13. Tables 5.14 and 5.15 show the power flow solution for CASE25 three phase unbalanced distribution by ϵDE-GN and υMAESbm, respectively. As shown in these tables, the voltage magnitudes and angles obtained by ϵDE-GN and υMAESbm are identical.

In Tables 5.14 and 5.15, it is to be noted that for bus 1 and bus 2, voltages and angles for all the phases are identical. This reason behind this as follows. When CASE25 system works in the grid connected mode, bus 1 acts as a root node connected to the

Table 5.12: Voltage profile obtained by υMAESbm for CASE33 distribution system operated as an islanded microgrid.

Bus	$\|V\|$	$\angle_V$	P	Q	$\|I\|$	$\angle_I$	Bus	$\|V\|$	$\angle_V$	P	Q	$\|I\|$	$\angle_I$	Bus	$\|V\|$	$\angle_V$	P	Q	$\|I\|$	$\angle_I$
1	–	–	–	–	–	-	12	0.9830	0.0003	-0.1200	-0.0700	0.1413	2.6138	23	0.9906	-0.0015	-0.1800	-0.1000	0.2079	2.6330
2	0.9922	0.0000	-0.2000	-0.1200	0.2351	2.6012	13	0.9773	-0.0011	-0.1200	-0.0700	0.1422	2.6124	24	0.9908	-0.0043	-0.8400	-0.4000	0.9390	2.6929
3	0.9909	-0.0001	-0.1800	-0.0800	0.1988	2.7233	14	0.9752	-0.0023	-0.2400	-0.1600	0.2958	2.5513	25	0.9944	-0.0064	0.4205	1.0644	1.1509	-1.2010
4	0.9905	0.0009	-0.2400	-0.1600	0.2912	2.5545	15	0.9738	-0.0029	-0.1200	-0.0200	0.1249	2.9736	26	0.9912	0.0051	3.0831	1.3764	3.4062	-0.4148
5	0.9906	0.0018	-0.1200	-0.0600	0.1354	2.6798	16	0.9725	-0.0033	-0.1200	-0.0400	0.1301	2.8166	27	0.9888	0.0060	-0.1200	-0.0500	0.1315	2.7528
6	0.9906	0.0043	-0.1200	-0.0400	0.1277	2.8241	17	0.9706	-0.0044	-0.1200	-0.0400	0.1303	2.8154	28	0.9779	0.0073	-0.1200	-0.0400	0.1294	2.8271
7	0.9901	0.0029	-0.4000	-0.2000	0.4517	2.6808	18	0.9701	-0.0046	-0.1800	-0.0800	0.2031	2.7188	29	0.9701	0.0085	-0.2400	-0.1400	0.2864	2.6220
8	0.9896	0.0022	-0.4000	-0.2000	0.4519	2.6801	19	0.9928	0.0002	-0.1800	-0.0800	0.1984	2.7236	30	0.9667	0.0102	-0.4000	-1.2000	1.3085	1.9027
9	0.9907	0.0010	1.3207	0.9988	1.6713	-0.6465	20	1.0000	0.0024	-0.1800	-0.0800	0.1970	2.7258	31	0.9627	0.0089	-0.3000	-0.1400	0.3439	2.7138
10	0.9853	0.0000	-0.1200	-0.0400	0.1284	2.8199	21	1.0024	0.0036	-0.1800	-0.0800	0.1965	2.7269	32	0.9618	0.0085	-0.4200	-0.2000	0.4837	2.7057
11	0.9845	0.0001	-0.0900	-0.0600	0.1099	2.5537	22	1.01	0.0063	1.4410	0.6	1.5769	-0.4285	33	0.9616	0.0084	-0.1200	-0.0800	0.1500	2.5620
w	0.9984																			

grid. However, when this system is working as an islanded microgrid, bus 1 becomes leaf node (Fig. 5.7) where as per the data specified, there are no load on bus 1 and bus 2. Hence no current flows between these buses in all the phases and due to this voltage magnitudes and angles for all phases at these buses shall be identical..

From the above discussion, it can be concluded that the performance of ϵDE-GN and υMAESbm is satisfactory on unbalanced islanded microgrids.

Table 5.13: Droop control settings of DGs in CASE25 test system.

DG	Location	S_p	S_q	ω^*	V^*	S_{max}	Q_{max}
1	13	0.005	0.05	1	1.01	0.6	0.36
2	19	0.01	0.1	1	1.01	0.3	0.18
3	25	0.005	0.05	1	1.01	0.6	0.18

5.8 Summary

In this chapter, novel algorithms for the power flow problem of an islanded microgrid are introduced. In proposed algorithms, the operating frequency is represented as an additional power flow variable. Various modes of DGs, droop, PV and PQ, are modeled as per the characteristics of islanded microgrids.

The proposed power flow problem is formulated as a constrained optimization problem which is solved by using two proposed algorithms, ϵDE-GN, and υMAESbm. The proposed algorithms are applied to balanced test systems: CASE6, CASE33, CASE69,

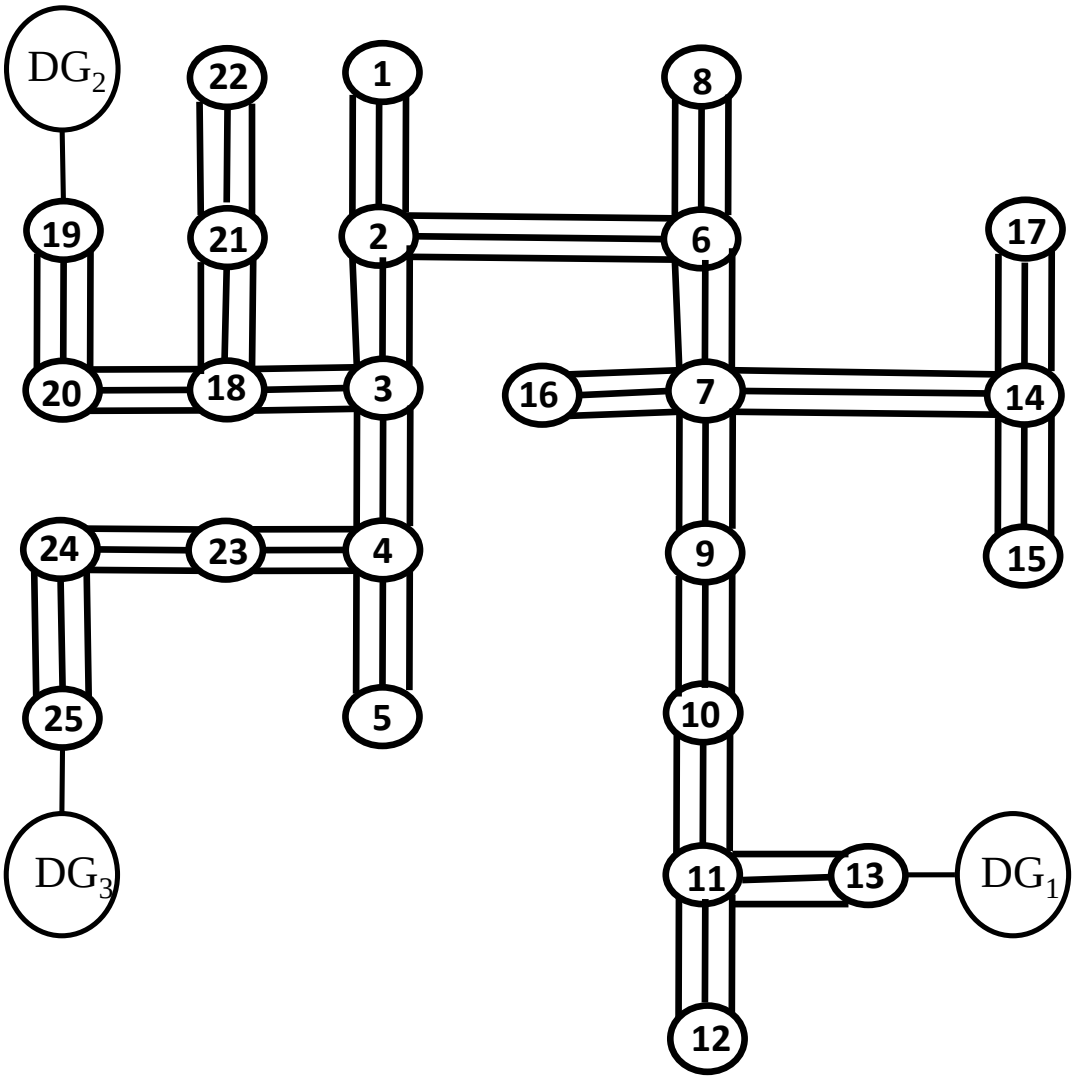

Figure 5.7: Topology of CASE25 test system operated as an islanded microgrid.

Table 5.14: Power flow result obtained by ϵDE-GN for CASE25 unbalanced distribution system operated as an islanded microgrid.

Bus	Phase a				Phase b				Phase c			
	$\|V\|$	$\angle_V$	P	Q	$\|V\|$	$\angle_V$	P	Q	$\|V\|$	$\angle_V$	P	Q
1	0.9894	0.0000	0.0000	0.0000	0.9893	-119.9860	0.0000	0.0000	0.9896	119.9868	0.0000	0.0000
2	0.9894	0.0000	0.0000	0.0000	0.9893	-119.9860	0.0000	0.0000	0.9896	119.9868	0.0000	0.0000
3	0.9901	0.0111	-0.0035	-0.0025	0.9899	-119.9791	-0.0040	-0.0030	0.9902	120.0002	-0.0045	-0.0032
4	0.9908	0.0320	-0.0050	-0.0040	0.9906	-119.9633	-0.0060	-0.0045	0.9908	120.0237	-0.0050	-0.0035
5	0.9904	0.0323	-0.0040	-0.0030	0.9902	-119.9621	-0.0040	-0.0030	0.9905	120.0233	-0.0040	-0.0030
6	0.9881	0.0039	-0.0040	-0.0030	0.9881	-119.9785	-0.0045	-0.0032	0.9885	119.9886	-0.0035	-0.0025
7	0.9876	0.0068	0.0000	0.0000	0.9876	-119.9723	0.0000	0.0000	0.9879	119.9913	0.0000	0.0000
8	0.9875	0.0046	-0.0040	-0.0030	0.9874	-119.9760	-0.0040	-0.0030	0.9879	119.9877	-0.0040	-0.0030
9	0.9892	0.0086	-0.0060	-0.0045	0.9893	-119.9762	-0.0050	-0.0040	0.9895	119.9981	-0.0050	-0.0035
10	0.9914	0.0101	-0.0035	-0.0025	0.9914	-119.9821	-0.0040	-0.0030	0.9914	120.0058	-0.0045	-0.0032
11	0.9929	0.0109	-0.0045	-0.0032	0.9929	-119.9867	-0.0035	-0.0025	0.9928	120.0112	-0.0040	-0.0030
12	0.9926	0.0113	-0.0050	-0.0035	0.9925	-119.9858	-0.0060	-0.0045	0.9925	120.0126	-0.0050	-0.0040
13	0.9953	0.0085	0.0393	0.0278	0.9953	-119.9915	0.0392	0.0286	0.9953	120.0085	0.0399	0.0284
14	0.9857	0.0076	-0.0050	-0.0035	0.9857	-119.9633	-0.0050	-0.0040	0.9860	119.9877	-0.0060	-0.0045
15	0.9850	0.0083	-0.0133	-0.0100	0.9850	-119.9608	-0.0133	-0.0100	0.9854	119.9869	-0.0133	-0.0100
16	0.9872	0.0072	-0.0040	-0.0030	0.9872	-119.9710	-0.0040	-0.0030	0.9876	119.9909	-0.0040	-0.0030
17	0.9853	0.0085	-0.0040	-0.0030	0.9854	-119.9627	-0.0035	-0.0025	0.9856	119.9882	-0.0045	-0.0032
18	0.9902	-0.0047	-0.0040	-0.0030	0.9900	-119.9959	-0.0040	-0.0030	0.9902	119.9881	-0.0040	-0.0030
19	0.9937	-0.0486	0.0159	0.0164	0.9937	-120.0486	0.0166	0.0178	0.9937	119.9514	0.0167	0.0168
20	0.9914	-0.0210	-0.0035	-0.0025	0.9913	-120.0168	-0.0040	-0.0030	0.9913	119.9774	-0.0045	-0.0032
21	0.9891	-0.0028	-0.0040	-0.0030	0.9888	-119.9932	-0.0035	-0.0025	0.9890	119.9915	-0.0045	-0.0032
22	0.9884	-0.0020	-0.0050	-0.0035	0.9880	-119.9912	-0.0060	-0.0045	0.9884	119.9943	-0.0050	-0.0040
23	0.9925	0.0394	-0.0060	-0.0045	0.9924	-119.9590	-0.0050	-0.0040	0.9925	120.0346	-0.0050	-0.0035
24	0.9947	0.0466	-0.0035	-0.0025	0.9945	-119.9563	-0.0045	-0.0032	0.9945	120.0462	-0.0040	-0.0030
25	0.9992	0.0527	0.0373	0.0241	0.9992	-119.9473	0.0387	0.0245	0.9992	120.0527	0.0384	0.0248
w	0.9993											

and unbalanced test systems: CASE25 test systems to analyze the performance of the algorithms. Moreover, the performance of the proposed algorithms is compared with the performance of PSO, GA, NTR, and time-domain software. The obtained results reveal that the performance of the proposed algorithm is superior to others.

Table 5.15: Power flow result obtained by υMAESbm for CASE25 unbalanced distribution system operated as an islanded microgrid.

Bus	Phase a				Phase b				Phase c			
	$\|V\|$	$\angle_V$	P	Q	$\|V\|$	$\angle_V$	P	Q	$\|V\|$	$\angle_V$	P	Q
1	0.9894	0.0000	0.0000	0.0000	0.9893	-119.9860	0.0000	0.0000	0.9896	119.9868	0.0000	0.0000
2	0.9894	0.0000	0.0000	0.0000	0.9893	-119.9860	0.0000	0.0000	0.9896	119.9868	0.0000	0.0000
3	0.9901	0.0111	-0.0035	-0.0025	0.9899	-119.9791	-0.0040	-0.0030	0.9902	120.0002	-0.0045	-0.0032
4	0.9908	0.0320	-0.0050	-0.0040	0.9906	-119.9633	-0.0060	-0.0045	0.9908	120.0237	-0.0050	-0.0035
5	0.9904	0.0323	-0.0040	-0.0030	0.9902	-119.9621	-0.0040	-0.0030	0.9905	120.0233	-0.0040	-0.0030
6	0.9881	0.0039	-0.0040	-0.0030	0.9881	-119.9785	-0.0045	-0.0032	0.9885	119.9886	-0.0035	-0.0025
7	0.9876	0.0068	0.0000	0.0000	0.9876	-119.9723	0.0000	0.0000	0.9879	119.9913	0.0000	0.0000
8	0.9875	0.0046	-0.0040	-0.0030	0.9874	-119.9760	-0.0040	-0.0030	0.9879	119.9877	-0.0040	-0.0030
9	0.9892	0.0086	-0.0060	-0.0045	0.9893	-119.9762	-0.0050	-0.0040	0.9895	119.9981	-0.0050	-0.0035
10	0.9914	0.0101	-0.0035	-0.0025	0.9914	-119.9821	-0.0040	-0.0030	0.9914	120.0058	-0.0045	-0.0032
11	0.9929	0.0109	-0.0045	-0.0032	0.9929	-119.9867	-0.0035	-0.0025	0.9928	120.0112	-0.0040	-0.0030
12	0.9926	0.0113	-0.0050	-0.0035	0.9925	-119.9858	-0.0060	-0.0045	0.9925	120.0126	-0.0050	-0.0040
13	0.9953	0.0085	0.0393	0.0278	0.9953	-119.9915	0.0392	0.0286	0.9953	120.0085	0.0399	0.0284
14	0.9857	0.0076	-0.0050	-0.0035	0.9857	-119.9633	-0.0050	-0.0040	0.9860	119.9877	-0.0060	-0.0045
15	0.9850	0.0083	-0.0133	-0.0100	0.9850	-119.9608	-0.0133	-0.0100	0.9854	119.9869	-0.0133	-0.0100
16	0.9872	0.0072	-0.0040	-0.0030	0.9872	-119.9710	-0.0040	-0.0030	0.9876	119.9909	-0.0040	-0.0030
17	0.9853	0.0085	-0.0040	-0.0030	0.9854	-119.9627	-0.0035	-0.0025	0.9856	119.9882	-0.0045	-0.0032
18	0.9902	-0.0047	-0.0040	-0.0030	0.9900	-119.9959	-0.0040	-0.0030	0.9902	119.9881	-0.0040	-0.0030
19	0.9937	-0.0486	0.0159	0.0164	0.9937	-120.0486	0.0166	0.0178	0.9937	119.9514	0.0167	0.0168
20	0.9914	-0.0210	-0.0035	-0.0025	0.9913	-120.0168	-0.0040	-0.0030	0.9913	119.9774	-0.0045	-0.0032
21	0.9891	-0.0028	-0.0040	-0.0030	0.9888	-119.9932	-0.0035	-0.0025	0.9890	119.9915	-0.0045	-0.0032
22	0.9884	-0.0020	-0.0050	-0.0035	0.9880	-119.9912	-0.0060	-0.0045	0.9884	119.9943	-0.0050	-0.0040
23	0.9925	0.0394	-0.0060	-0.0045	0.9924	-119.9590	-0.0050	-0.0040	0.9925	120.0346	-0.0050	-0.0035
24	0.9947	0.0466	-0.0035	-0.0025	0.9945	-119.9563	-0.0045	-0.0032	0.9945	120.0462	-0.0040	-0.0030
25	0.9992	0.0527	0.0373	0.0241	0.9992	-119.9473	0.0387	0.0245	0.9992	120.0527	0.0384	0.0248
w	0.9993											